JCTC Journal of Chemical Theory and Computation

Article

pubs.acs.org/JCTC

Bridging Static and Dynamical Descriptions of Chemical Reactions: An *ab Initio* Study of CO_2 Interacting with Water Molecules

Grégoire A. Gallet,[†] Fabio Pietrucci,[†] and Wanda Andreoni*[,†,‡]

[†]Centre Européen de Calcul Atomique et Moléculaire (CECAM), Ecole Polytechnique Fédérale de Lausanne, Switzerland

[‡]Institut de Théorie des Phénomènes Physiques, Ecole Polytechnique Fédérale de Lausanne, Switzerland

Supporting Information

ABSTRACT: Extracting reliable thermochemical parameters from molecular dynamics simulations of chemical reactions, although based on ab initio methods, is generally hampered by difficulties in reproducing the results and controlling the statistical errors. This is a serious drawback with respect to the quantum-chemical description based on potential energy surfaces. This work is an attempt to fill this gap. We apply molecular dynamics, based on density functional theory (DFT) and empowered by path metadynamics (MTD), to simulate the reaction of CO_2 with (one, two, and three) water molecules in the gas phase. This study relies on a strategy that ensures a precise control of the accuracy of the reaction coordinates and of the reconstructed free-energy surface on this space, namely, on (i) fully reversible MTD simulations, (ii) a committor probability analysis for the diagnosis of the collective variables, and (iii) a cluster analysis for the characterization of the reconstructed free-energy surfaces. This robust procedure permits a meaningful comparison with more traditional calculations of the potential energy surfaces that we also perform within the same DFT computational scheme. This comparison shows in particular that the reactants and products of systems with only three water molecules can no longer be understood in terms of one structure but must be described as statistical configuration ensembles. Calculations carried out with different prescriptions for the exchange-correlation functionals also allow us to establish their quantitative effect on the activation barriers for the formation and the dissociation of carbonic acid. Their decrease induced by the addition of one water molecule (catalytic effect) is found to be largely independent of the specific functional.

1. INTRODUCTION

The reaction of carbon dioxide (CO_2) with water in various phases is of fundamental importance in diverse fields of chemistry, ranging from biochemistry to environmental chemistry. In particular, its role is crucial in many of the routes in use or being explored for the capture and sequestration of CO_2.[1−3] This explains the renewed and ever growing interest in characterizing the interaction of CO_2 with water at the microscopic level.[4,5] Theory and computations could be highly relevant in these studies, because of the difficulty in experiments to observe the various steps of these reactions.

The path toward this target is by far not straightforward. On one hand, characterization and understanding of molecular reactions is rooted in well-established theories (see, e.g., ref 6−8) also dealing with nuclear quantum effects;[9−12] on the other, the complexity of the real systems calls for efficient approaches, thus implying other approximations. The study of chemical reactions in condensed phases, especially in solution, has long been pursued within hybrid schemes with the "solvent" modeled as a continuum.[13] The inclusion of density functional theory (DFT) in molecular dynamics (MD)[14] has marked an important step forward for the investigation of physical and chemical processes in condensed matter systems.

Nowadays, the typical approach to the study of chemical reactions in condensed phases uses DFT-MD, which has recently been empowered by accelerated sampling methods like metadynamics.[15−17] Although partial studies of CO_2 in solution have already been made using metadynamics simulations,[18−20] a number of issues remain open which must be solved before applying these techniques with confidence to predict the physical behavior of CO_2−water systems.

In particular, we should be able to answer the following questions: (i) to what extent do the available implementations of DFT "correctly" describe these systems, and (ii) to what extent can we rely on the characterization of the free-energy surface (FES) from a DFT metadynamics-based simulation at finite temperature? In other words, is the robustness of this method comparable to that of the computations of the potential energy surface (PES) for the same reactions? In this paper, we investigate both i and ii questions by studying the association and dissociation reactions

$$CO_2 + nH_2O \rightarrow H_2CO_3 + (n-1)H_2O \quad (1)$$

(n = 1,2,3) in the gas phase in a systematic way: We use several exchange-correlation (xc) functionals and, within the same computational schemes, determine local minima and transition states of the potential energy surface (PES) and of the room-temperature (RT) free-energy surface (FES).

Investigating the reactions in eq 1 in the gas phase gives us the opportunity to make a one-to-one comparison of our DFT results for the PES features with those of high-level post-Hartree−Fock approaches,[21−26] like Møller−Plesset second-order perturbation theory (MP2), quadratic configuration-interaction, and coupled-cluster theory. On the other hand, the characterization of the FES we present here is unprecedented: it

Received: July 7, 2012
Published: August 22, 2012

is obtained via DFT-based path metadynamics,[27] and process reversibility is achieved, which ensures the convergence of the reconstructed FES. Moreover, we use the clustering approach to categorize the FES basins and identify the "cluster" configurations in each of them, and we compute committor probabilities[28] mainly to verify our assignment of transition states. We will show, in particular, that simple collective variables (e.g., ref 29) are not appropriate for metadynamics simulations of the reactions of eq 1 in the gas phase. Finally, comparison between the computed features of the PES and the FES will allow us to gain insight into other important aspects of the reactions (eq 1) and, in particular, to resolve the question: (iii) to what extent is a calculation of the PES sufficient to describe the salient features of these processes? In particular, our analysis will lead us to estimate the contribution of entropy to reaction barriers and compare it with more traditional calculations that include a separate estimation of the rotational, translational, and vibrational components, with the latter computed either in the harmonic or quasi-harmonic approximation.

The methodological problems we discuss and solve in this paper are of general interest in the study of chemical reactions. By focusing on an important case, already studied with high-level quantum mechanical approaches, our intention is to establish a new protocol for the application and interpretation of state-of-the-art DFT-based simulations of the dynamics of molecular reactions.

2. RESULTS AND DISCUSSION

2.1. DFT-Based Calculations: The Potential Energy Surface. The study of the reactions in eq 1 commonly reduces to the determination of the stationary points (minima and saddle points) of the PES: reactants (R_n), products (P_n), and transitions states (TS_n). There is full consensus among the results of post-Hartree–Fock methods[22−26] about the existence of very weakly bound reactants (preassociation complexes), the nature of the transition states, and the catalytic role of water molecules in the formation and dissociation of carbonic acid as well as in the trends in binding energies and barrier heights. However, significant differences in the energetics are found, depending on the level of theory and also on the choice of the basis set for the wave functions.

In this section, we present the results of a series of calculations performed with different DFT schemes (PBE, BLYP, B3LYP) using the pseudopotential description of the core–valence interaction. For a direct verification of the pseudopotentials, we performed B3LYP calculations also in the traditional all-electron implementation of quantum-chemical codes. Moreover, within this same all-electron scheme, we made calculations using the hybrid M06 functional. (Detailed information on our calculations is given in section 4). In this way, we can explore possible discrepancies between the predictions of functionals widely employed in the quantum–chemical description of molecules. Next, we compare our DFT results with those of the MP2 and coupled-clusters methods,[25] the latter relying on the MP2 geometries and vibrational spectra.

Figure 1 illustrates a sketch of the configurations of the reactants, transition states, and products of eq 1. Geometrical parameters are given in Table 1 of the Supporting Information (SI). The T-shaped structure of R_1 evolves into cyclic conformations for the reactants with an increasing number of water molecules, all having one oriented relative to CO_2 as in R_1. The TSs consist of four-, six-, and eight-member rings for n = 1, 2, and 3, respectively. In the n = 3 case, following previous studies,[23,25,30] we considered two types of reactants, differing in the configuration of the water trimer (either closed (R_3) or open (R'_3)). These lead to different configurations for the hydrated carbonic acid (P_3 or P'_3) and different reaction paths.

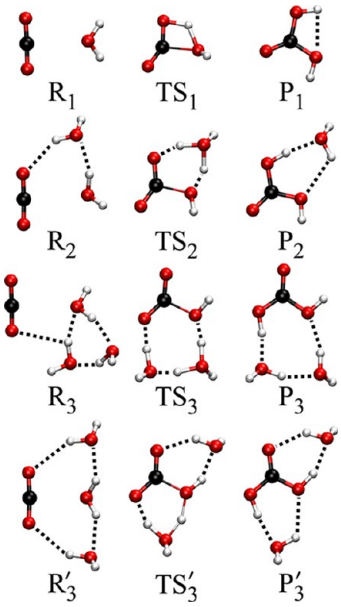

Figure 1. Reactants, products, and transition states for the reactions in eq 1 (n = 1–3).

Table 1 contains the results obtained for binding energies relative to the isolated molecules. Tables 2 and 3 report the values of the barrier heights ($E(TS_n) - E(R_n)$ and $E(TS_n) - E(P_n)$, respectively) and also the change due to the addition of one water molecule.

Several remarks follow from the inspection of our results:

- The structures of the reactants, transition states and products of the reactions in eq 1 do not differ significantly on passing from one functional scheme to the other. Changes relative to the MP2 geometries[25] are also minor (see Table 1 in the SI).
- The PES is flat around the local minima corresponding to the preassociation complexes R_n. For example, in the case n = 1, the value of the binding energy of the T-shaped complex is even lower than the accuracy of the calculations (see Table 1), variations of 0.1 Å in d_1 change the energy by less than 0.1 kcal/mol, and vibrational eigenmodes, which primarily involve the variation of this distance, have frequencies lower than 150 cm^{-1}. The increase of binding energy with increasing n is mainly due to the formation of hydrogen bonds between the water molecules (see results for the water dimer and trimer in Table 2 of the Supporting Information).
- PBE appears to have a lower global performance relative to the other functionals. This is not surprising, being nonempirical and thus, in particular, not tailored to molecular systems. The good agreement between PBE and CCSD(T) in predicting the binding energies of both reactants and products relative to the isolated H_2O and CO_2 molecules can hardly be considered a (kcal/mol) consequence of the correct description of these systems. Rather, it can be seen as a manifestation of the tendency of PBE to strengthen intermolecular bonds (relative to e.g. BLYP), which leads to an accurate account of

dx.doi.org/10.1021/ct300581n | J. Chem. Theory Comput. 2012, 8, 4029–4039

Table 1. Binding Energies (kcal/mol) Referred to the Isolated CO_2 and H_2O molecules, Including Zero-Point Energy (ZPE)

system	PBE[a]	BLYP[a]	B3LYP[a]	B3LYP[b]	M06[b]	MP2[c]		CCSD(T)[d]	
R_1	−1	abs <1	abs <1	−1	−2	*−2.0*	[−1.9]	*−2.1*	[−2.0]
TS_1	40	46	49	48	49	*48.3*	[49.1]	*48.5*	[49.4]
P_1	8	14	11	10	11	*11.4*	[*11.5*]	*8.6*	[*8.5*]
R_2	−6	−3	−4	−4	−6	*−7.0*	[−6.6]	*−7.2*	[−6.7]
TS_2	16	25	26	26	26	*25.1*	[26.0]	*25.0*	[26.0]
P_2	2	9	6	5	4	*4.2*	[*4.6*]	*1.6*	[*1.7*]
R_3	−12	−8	−9	−10	−12	*−14.2*	[−13.5]	*−14.4*	[−13.6]
TS_3	5	16	15	15	15	*14.0*	[15.2]	*13.9*	[15.2]
P_3	−6	3	−1	−1	−2	*−3.0*	[−2.2]	*−5.7*	[*−4.9*]
R'_3	−9	−5	−7	−7	−9	*−10.9*	[−10.2]	*−11.3*	[−10.5]
TS'_3	6	18	17	17	16	*14.3*	[15.3]	*13.8*	[15.0]
P'_3	−9	2	−3	−4	−6	*−5.6*	[*−5.1*]	*−8.5*	[*−7.9*]

[a]This work: Pseudopotential-plane waves up to 100 Ry cutoff. [b]This work: AE-aug-cc-pVTZ. [c]Ref 25: AE-aug-cc-pVTZ. Within brackets: values extrapolated to the complete basis set (CBS) limit. Values reported in the Supporting Information are in italics. [d]Ref 25: basis sets as in c; single-point calculations on MP2 geometries.

Table 2. Enthalpy Barrier Height in (kcal/mol) for the Formation of Carbonic Acid and Its Decrease (in Italics) Due to the Addition of One Water Molecule (from *n* to (*n* + 1); Labels as in Table 1)

n	PBE[a]	BLYP[a]	B3LYP[a]	B3LYP[b]	M06[b]	MP2[c]	CCSD(T)[d]
1	41	46	49	49	51	50	51
2	22	29	30	30	32	32	32
1−2	*19*	*18*	*19*	*19*	*19*	*18*	*19*
3	17	24	25	25	28	28	28
2−3	*5*	*5*	*5*	*5*	*4*	*4*	*4*
3′	15	23	23	24	25	25	25
2−3′	*7*	*5*	*6*	*6*	*7*	*7*	*7*

Table 3. Enthalpy Barrier Height (in kcal/mol) for the Dissociation of Carbonic Acid and Its Decrease (in Italics) Due to the Addition of One Water Molecule (from *n* to (*n* + 1); Labels as in Table 1)

n	PBE[a]	BLYP[a]	B3LYP[a]	B3LYP[b]	M06[b]	MP2[c]	CCSD(T)[d]
1	32	32	37	38	39	37	40
2	15	16	20	21	22	21	23
1−2	*17*	*16*	*17*	*17*	*17*	*16*	*17*
3	11	12	17	16	18	17	20
2−3	*4*	*4*	*4*	*4*	*4*	*4*	*4*
3′	15	17	20	21	21	20	22
2−3′	abs < *1*	abs < *1*	*1*	abs < *1*	*1*	*1*	*1*

the hydrogen bonds in the water dimer and trimer[31] but also explains the too high stabilization of the TS (by about 10 kcal/mol).

- On passing from BLYP to B3LYP, a sizable change is found only in the binding energy of the carbonic acid (Table 1), which is reflected in all products (*n* = 2 and 3 in Table 1). The improvement of the barrier heights is also evident. In principle, this comparison should clarify the effect of correcting the semilocal BLYP exchange by introducing a certain contribution of exact exchange, but the simultaneous empirical modification of the relative weight of the LYP correlation term does not allow for a "clean" interpretation.
- Additional calculations in the BLYP-D[32,33] approximation for the xc-functional, which includes empirical corrections for van-der-Waals interactions (see Table 3 of the SI), show that, although improving on the binding energies, they have no effect on the barriers.
- Comparison of the two sets of B3LYP calculations, in the pseudopotential and all-electron approaches, shows the accuracy of the former.
- There is close agreement between M06 and B3LYP for all calculated values. Moreover, these results are very close to the MP2 results.[25]
- All methods predict the same values for the ZPE contributions to energy differences within ∼1 kcal/mol (see Table 4 of the SI): in particular, an increase of the energy of the product complexes relative to the isolated molecules ranging from 4 (*n* = 2) to 8 (*n* = 3) kcal/mol and a decrease of the barrier heights for both formation and dissociation of carbonic acid, of only 1−2 kcal/mol for the former and of 3−4 kcal/mol for the latter, independent of the number of water molecules.
- All xc-functionals considered here (GGA, hybrid, and meta-hybrid) give the same quantitative account of the catalytic effect (within 1 kcal/mol), which also fully agrees with the prediction of MP2 and CCSD calculations (Tables 2 and 3). This is an interesting result and suggests that electrostatic effects provide the dominant contribution to the catalyzing function of an additional water molecule, both for the formation and the dissociation of carbonic acid.

dx.doi.org/10.1021/ct300581n | J. Chem. Theory Comput. 2012, 8, 4029−4039

2.2. DFT-Based Metadynamics: The Free Energy Surface. In this section, we study the reactions in eq 1 with DFT-based MD simulations carried out within the PBE, BLYP, and B3LYP functional schemes. All simulations are performed in the *NVT* ensemble at 300 K.

Given the size of the barriers found in section 2.1, it is compelling to accelerate the occurrence of the reactions using an enhanced sampling algorithm like metadynamics.[15] While referring to section 4 for the relevant definitions and computational details, here we discuss the choice of the collective variables and care, explaining how we validate our calculations, because this step is crucial and unprecedented. Then, we discuss the characteristics of the room-temperature FES and in particular our findings for the FES basins and barriers of interest.

2.2.1. Choice of CVs. The first step of a MTD simulation is the selection of suitable collective variables (CVs) and deserves special care because unsuitable CVs may hamper identifying the correct transition states and affect the validity of the reconstructed FES through hysteresis.[34,35] This choice is a crucial issue for all methods based on dimensional reduction, i.e., not only MTD but also, e.g., umbrella sampling, thermodynamic integration, and steered molecular dynamics. Traditionally, simple analytic functions of the atomic coordinates are adopted like distances, coordination numbers, and angles. However, other more powerful CVs may become necessary. This is the case of the reactions in eq 1, which imply concerted pathways involving several atoms and thus require more sophisticated and especially flexible CVs. This led us to choose path metadynamics,[27] as described in section 4.2. We underline here that the exploration can start from an initial putative reaction pathway and is in no way confined to predefined configurations for either transition or intermediate states.[36] An important practical consequence is that a change in the setup such as the xc-functional or the temperature does not imply fine-tuning of the sampling procedure.

As detailed in section 4.2, in our first attempt to investigate the kinetics of the reactions in eq 1 for $n = 1$, we employed traditional CVs, namely, the number of C−O−H covalent "bridges" and the C−O coordination number within 4 Å. In this way, we could simulate both association and dissociation reactions. However, despite extensive fine-tuning of the CVs, the analysis of the trajectories revealed different TSs for the forward and backward reactions, which suggested the occurrence of hysteresis. Moreover, both configurations were sizably different from the one obtained for the TS in section 2.1, and the FE barriers derived from the reconstructed FES were 20 kcal/mol higher than those calculated on the PES. Such a result could not be explained in terms of entropic contributions to the FE barriers. On the other hand, the failure of the simple CVs could be traced back to the concerted nature of the reactions.

We remark that the dissociation of gas-phase carbonic acid was studied in ref 29 also using DFT-based MTD, in the BLYP approximation of the xc-functional. Traditional CVs were adopted, namely, the C−O and O−H coordination numbers. However, no attempt was reported to validate this choice and the reconstructed FES. Specific comments will be made below on the basis of our results.

2.2.2. Verification of the FES Accuracy. Before presenting our results for the FES reconstructed from the MTD trajectories, we discuss how we have validated our scheme and thus established its robustness. In the study of chemical reactions with DFT-based metadynamics, it is customary to estimate the free-energy barrier from the bias potential accumulated after a single barrier-crossing event. This is also the case for any previous simulations of the reactions in eq 1 either in the gas[29] or the liquid phase.[18−20] Generally, no attempt is made to assess the statistical convergence of these calculations, and even the very requirement of fully reversible reactions is often unmet. This is what we have achieved here for each of the systems examined:

- Within the span of each simulation (about 200 ps), we could observe ∼10 forward/backward reactions: the reversibility of the dynamics allowed us to assess the

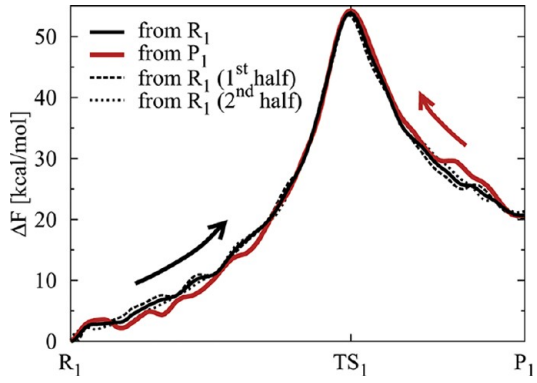

Figure 2. Free energy profile along the reaction path for the reaction in eq 1 with $n = 1$ (BLYP): from reactant (solid black) and product (solid red) and from the two halves of the path started from the reactant (dashed and dotted black lines).

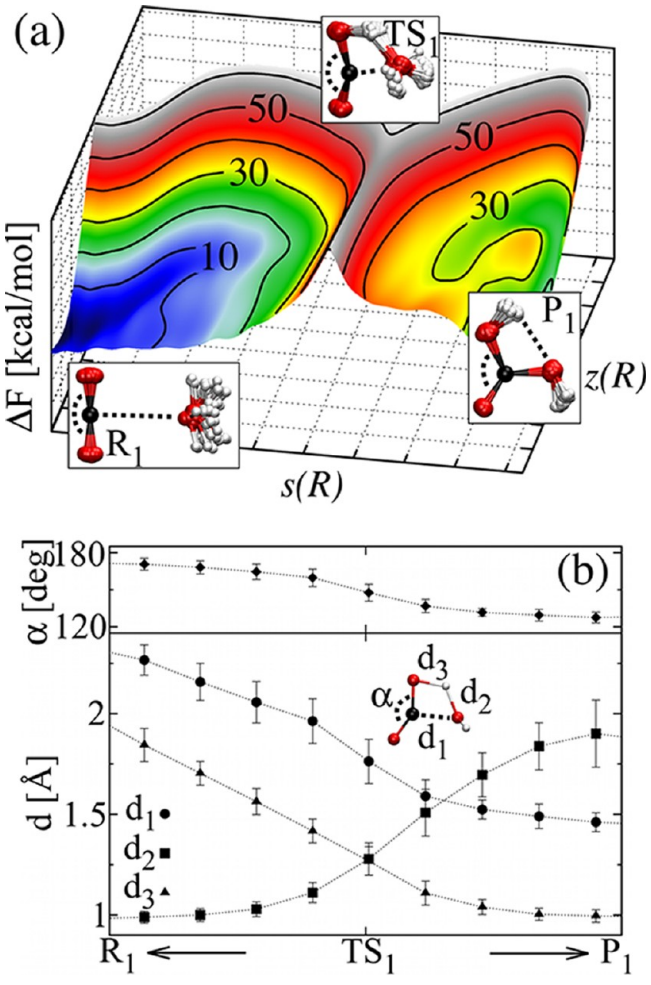

Figure 3. $n = 1$: (a) Free energy surface for the reactions in eq 1 and (b) evolution of relevant distances along the reaction pathway (BLYP). Distances in Å and angles in degrees. Error bars denote the RMSD.

dx.doi.org/10.1021/ct300581n | J. Chem. Theory Comput. 2012, 8, 4029−4039

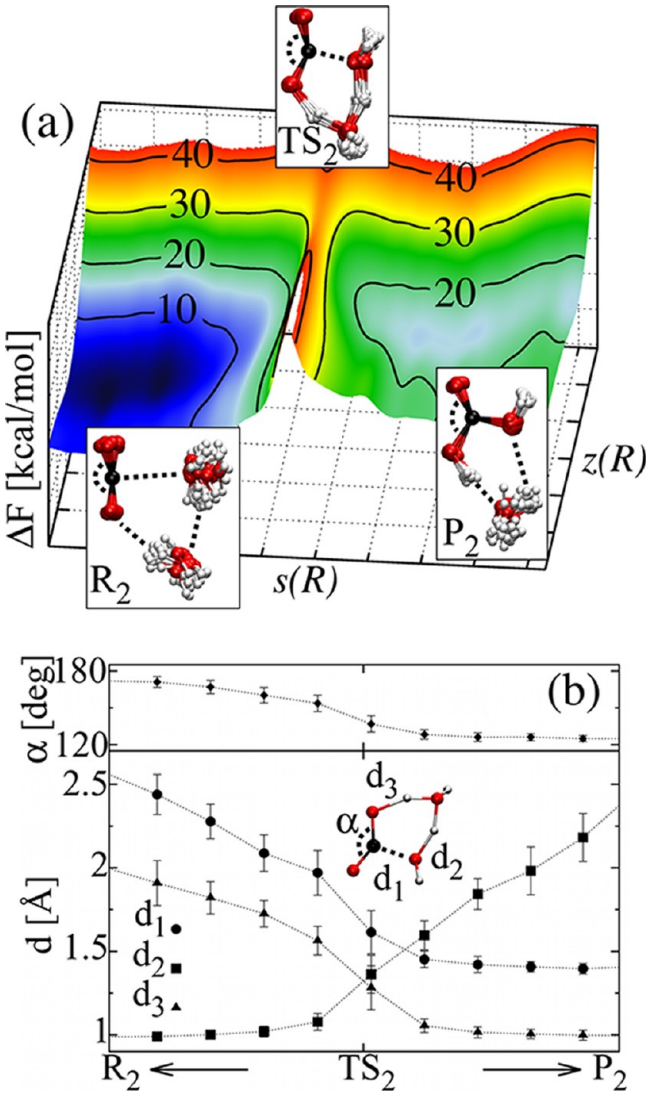

Figure 4. $n = 2$: (a) Free energy surface for the reactions in eq 1 and (b) evolution of relevant distances along the reaction pathway (BLYP). Details as in Figure 3.

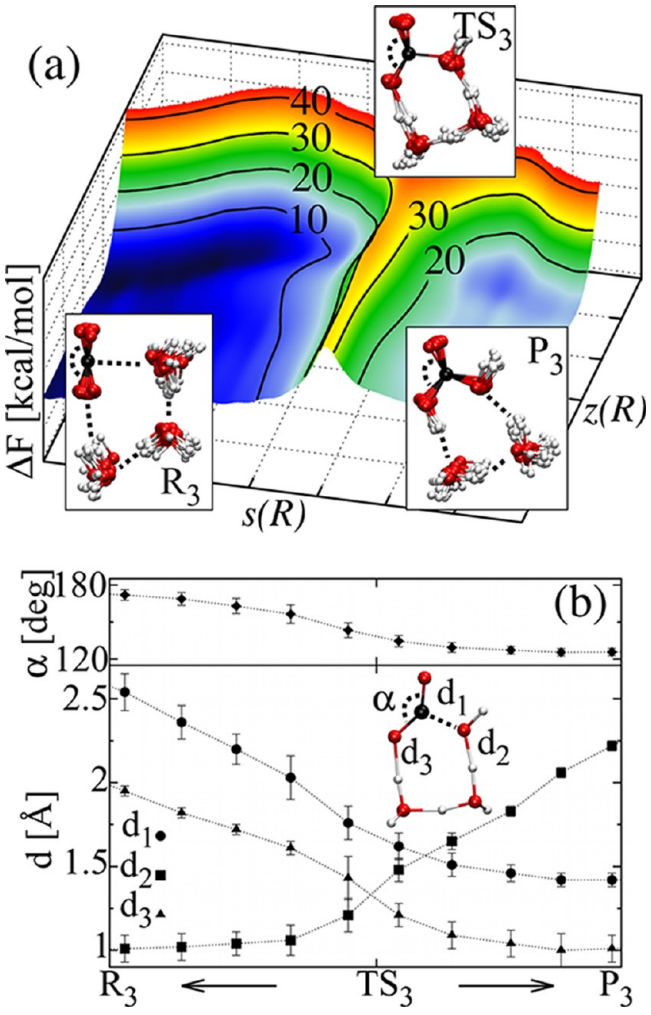

Figure 5. $n = 3$: (a) Free energy surface for the reactions in eq 1 and (b) evolution of relevant distances along the reaction pathway (BLYP). Details as in Figure 3.

statistical convergence of our FES within 2 kcal/mol. We emphasize that the FES, and its profile along the reaction path in particular, grew parallel to itself for about 100 ps after the "filling time". The possibility of hysteresis originating from missing relevant reaction coordinates is thus very unlikely. Figure 2 plots our findings for $n = 1$.

- We verified the reproducibility of our results by performing two independent simulations starting from either the reactants or the reaction products. Excellent agreement over the whole FES was found, with an average deviation lower than 2 kcal/mol. The results for $n = 1$ are illustrated in Figure 2. The same convergence quality was obtained in all simulated reactions, namely for all systems and all xc-functionals investigated (see Figure 1 of the SI).

2.2.3. FES Landscape and Comparison with the PES. We now turn with confidence to the inspection of the FES, and in particular to the characterization of the basins, the description of the dynamics of the reactions of eq 1, and the calculation of the free-energy barriers.

Figures 3a, 4a, 5a, and 6a represent the free-energy surfaces in the path-CV space. These results refer to the BLYP calculations. Plots corresponding to the other xc functionals are reported in the SI (see Figure 2 of the SI). To clarify the conformational changes taking place over the reaction path, the evolution of selected distances is plotted in Figures 3b, 4b, 5b, and 6b.

A. Cluster Analysis. The first step of our analysis is the inspection of the FES basins, that, as mentioned above, were delimited within a window of 3 kcal/mol. In the systems with one and two water molecules, the cluster analysis (see section 4.2) confirms the characteristics of the stationary points identified in the PES. The TS regions are represented by single clusters with structures closely reflecting those of TS_1 and TS_2 in Figure 1. The reactant and product basins comprehend more clusters; however, the geometries are close to those at the PES minima (R_1, R_2, P_1, and P_2 in Figure 1) and differ among each other mainly in the relative orientations of the water molecules. The "dynamic" conformations of the reactants are less compact than those of the products. These results are in agreement with the peculiar flatness of the PES around the R_1 and R_2 minima (section 2.1).

In the case of systems with three molecules, we have performed two distinct series of simulations starting from the two reaction paths (R_3−TS_3−P_3) and (R'_3−TS'_3−P'_3) identified in section 2.1. We remark that multiple reaction pathways can be observed in a single simulation of this type; however, the

dx.doi.org/10.1021/ct300581n | J. Chem. Theory Comput. 2012, 8, 4029−4039

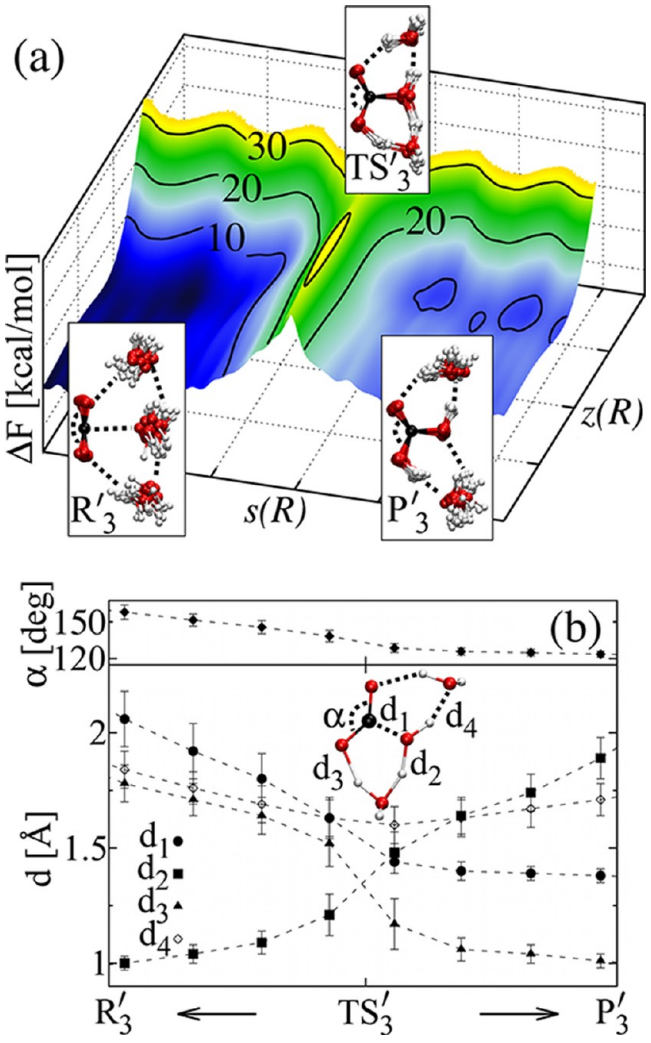

Figure 6. n = 3′: (a) Free energy surface for the reactions in eq 1 and (b) evolution of relevant distances along the reaction pathway (BLYP). Details as in Figure 3.

approach we have chosen allows for a more precise characterization of each one.

For the first reaction (R_3–TS_3–P_3), the cluster analysis reveals that the reactant basin can be described as a continuum of fluctuating conformers with sizable geometrical discrepancies, as can be seen in Figure 7a, showing the centers of the

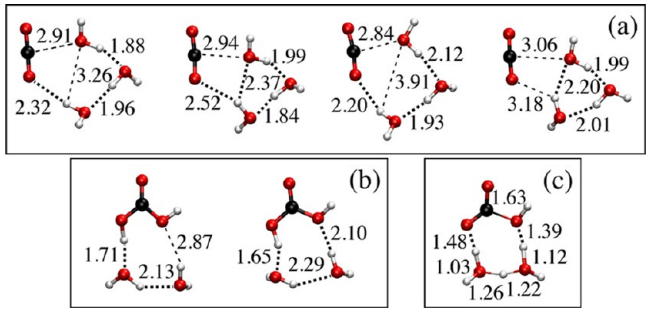

Figure 7. n = 3: Cluster centers for the (a) reactant basin, (b) product basin, and (c) TS region. Distances in Å.

four most populated clusters (covering 70% of the ensemble of 1100 configurations). Most of the time, CO_2 keeps one H bond

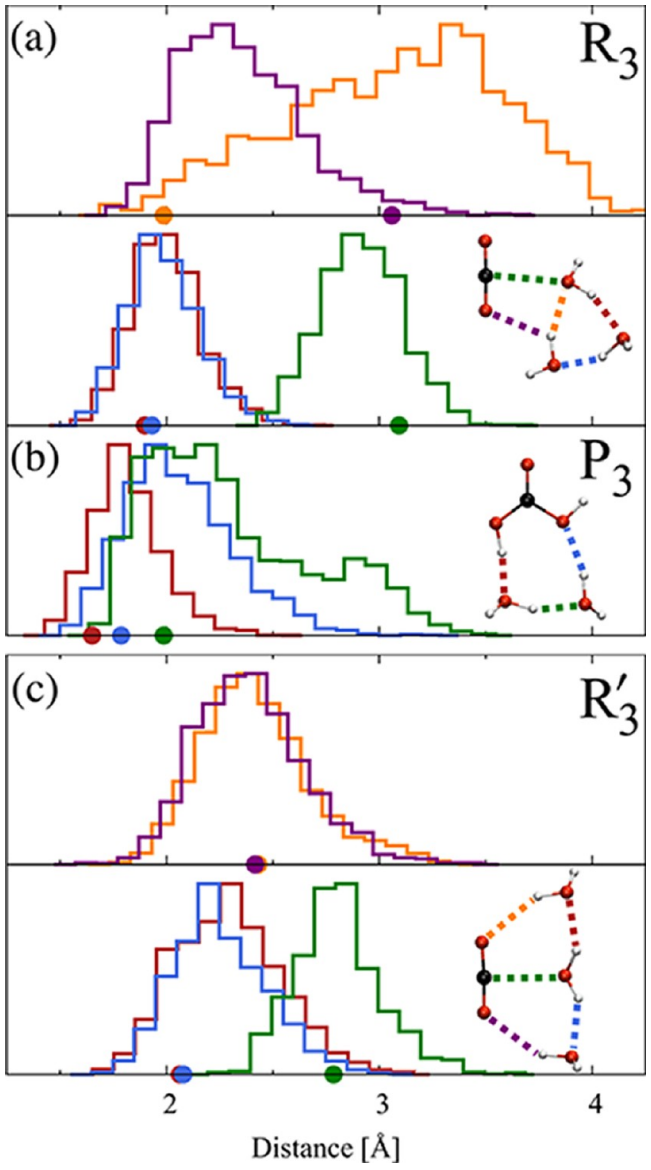

Figure 8. n = 3,3′: Distribution of relevant distances in the reactant and product basins.

Table 4. n = 1 and 2: Free-Energy Barrier Height in (kcal/mol) for the Formation and Dissociation of Carbonic Acid at Room Temperature and Decrease (in Italics) Due to the Addition of One Water Molecule (from n = 1 to n = 2)

	formation			dissociation			
n	PBE	BLYP	B3LYP	PBE	BLYP	B3LYP	n
1	46	51	54	31	33	38	1
2	29	32	31	18	20	19	2
1–2	*17*	*20*	*23*	*14*	*13*	*19*	*1–2*

with the water complex that fluctuates between a closed trimer and an open chain, but it also appears as in the structure of the PES minimum, namely more weakly bound to the water moiety (right side of Figure 7a). Using the same cutoff as for the reactants, clustering shows a narrower distribution for the product basins (two clusters cover 85% of 1600 configurations, see Figure 7b) and especially for the "transition state" that reduces to a single cluster (Figure 7c; the number of structures is however inherently small, only 70). Products mainly consist

dx.doi.org/10.1021/ct300581n | J. Chem. Theory Comput. 2012, 8, 4029–4039

Table 5. n = 1 and 2: Enthalpy Barrier Heights (in kcal/mol) for the Formation and Dissociation of Carbonic Acid Estimated from Room-Temperature DFT-MD and Barrier Decrease (in Italics) Due to the Addition of One Water Molecule[a]

formation				dissociation			
n	PBE	BLYP	B3LYP	PBE	BLYP	B3LYP	n
1	42[41]	48[47]	50[50]	33[34]	34[35]	38[41]	1
2	24[23]	31[30]	31[31]	17[17]	19[16]	22[17]	2
1−2	*18[19]*	*17[18]*	*20[19]*	*16[17]*	*15[16]*	*16[17]*	*1−2*

[a]In square brackets: result from the PES calculations (70 Ry).

of a carbonic acid interacting with a water dimer via one or two hydrogen bonds. As further illustration of the nature of the FES basins, Figure 8 gives an overview of the distribution of relevant distances measured in the reactant and product regions and provides a measure of the deviation with respect to the T = 0 structures (distance values marked with circles). The complexity is confirmed. In particular, Figure 8 clarifies again that while the T = 0 structure of the reactant consists of a water trimer bound to the carbon dioxide molecule, at room temperature the chain of H bonds opens up and becomes more prone to dissociation.

The second series of simulations (R_3−TS'_3−P'_3) leads to a different FES landscape. Here, the histogram of the relevant distances (in Figure 8) shows that the reactant basin is more compact and the centers of the distribution are close to the T = 0 values. These findings are confirmed by the cluster analysis (see Figure 3 of the SI): The most populated clusters consist of a chain of three water molecules, of which two are H-bonded to CO_2 and bridged by the third one. The product basin is essentially encompassed by four closely related clusters (90%), all showing carbonic acid hydrogen-bonded to two separate water molecules. The TS region is again narrow and reduces to one cluster reflecting the TS configuration determined on the PES.

B. Free-Energy Surface vs Potential Energy Surface. The free-energy barriers calculated for the formation and dissociation reactions in eq 1 are reported in Tables 4 and 6. For the cases with n = 3, we restrict our study to the PBE and BLYP schemes.

The result published by Kumar et al.[29] for the dissociation barrier of carbonic acid in the absence of water molecules is 37 kcal/mol from BLYP calculations: the 4 kcal/mol discrepancy with our BLYP value can easily be traced back to the different *ab initio* setup (pseudopotential, box size, etc.), and to the different MTD protocol. As discussed in section 2.2.1, in ref 29 an ad-hoc definition was adopted for the CVs, and a standard procedure was followed to estimate the FES, namely, one based on the MTD bias accumulated up to the first transition event, that was not validated by the parallel growth of the FES within reversible reactive trajectories.

Comparison of the FES and PES barriers provides further important information on the reactions of eq 1. Still, care must be taken that the values we estimate for the former have statistical uncertainties (∼2 kcal/mol as estimated in section 2.2.2).

Within the accuracy of the calculations, the variations due to the specific xc functional approximation are essentially the same as discussed in section 2.1. The catalytic effect of one additional water from n = 1 to n = 2 decreases slightly and is still rather independent of the xc functional; however, on passing from n = 2 to n = 3 there are more sizable differences. In order to better quantify these discrepancies, we estimated the enthalpy barriers from the Kohn−Sham total energies accumulated during the dynamics. After wave function optimization applied to 13 000 frames, we have a posteriori verified that the deviation from the Born−Oppenheimer surface leads to an error of ∼2 kcal/mol

Table 6. n = 3,3′: Free-Energy Barrier Heights in (kcal/mol) for the Formation and Dissociation of Carbonic Acid[a]

formation			dissociation		
n	PBE	BLYP	PBE	BLYP	n
3	26	31	16	19	3
2−3	*3*	*1*	*1*	*1*	*2−3*
3′	19	26	15	16	3′
2−3′	*10*	*6*	*3*	*4*	*2−3′*

[a]Decrease (in italics) due to the addition of one water molecule.

Table 7. n = 3,3′: Enthalpy Barrier Heights in (kcal/mol) for the Formation and Dissociation of Carbonic Acid, Calculated from Room-Temperature DFT-MD[a]

formation			dissociation		
n	PBE	BLYP	PBE	BLYP	n
3	20 [18]	28 [26]	13 [14]	17 [16]	3
2−3	*4 [4]*	*3 [4]*	*4 [4]*	*2 [4]*	*2−3*
3′	16 [15]	24 [23]	19 [17]	18 [20]	3′
2−3′	*8 [8]*	*8 [6]*	*−2 [abs < 1]*	*1 [abs < 1]*	*2−3′*

[a]Decrease (in italics) due to the addition of one water molecule. In square brackets: results from the PES calculations (70 Ry).

on these values. It is also important to note that they do not contain the ZPE contribution (a precise comparison is added in Tables 5 and 7). The agreement within the error bars is remarkable in all cases. This gives us confidence in ascribing the differences found in the cases of three molecules mainly to the influence of the entropic term of the free energy. This is consistent with the peculiar nature of the reactant and product FES basins described above, which cannot be described in terms of a single cluster as for the n = 1 and n = 2 systems.

An estimate of the entropy contribution to the free-energy barriers can thus be obtained from eq 11, which implies errors of the order of 3 kcal/mol. In a traditional quantum-chemical approach, the entropy term is obtained by evaluating the vibrational entropy in either the harmonic or the quasi-harmonic approximation,[37] and adding translational and rotational entropy terms. Our results are reported in Table 6 of the SI, compared with those relative to the MP2 geometries.[25] We recall that our DFT-MD simulations do not include nuclear quantum effects; therefore comparison can be made with the classical expression in which normal modes are populated according to Boltzmann distribution (see Table 8). Differences are negligible for n = 1 but start to be sizable already for n = 2.

At this point, a question arises about the dependence of the free-energy barrier on temperature. Additional BLYP simulations at T = 500 K for $CO_2 + H_2O \leftrightarrow H_2CO_3$ resulted in insignificant changes for the dissociation reaction (within 1−2 kcal/mol) but in a sizable increase (by 6 kcal/mol) for the formation reaction, mainly due to an increase of the TS_1−R_1 entropy difference (the reactant becomes more "disordered").

dx.doi.org/10.1021/ct300581n | J. Chem. Theory Comput. 2012, 8, 4029−4039

Table 8. Entropy Contribution $T\Delta S$ to the Free-Energy Barriers at Room-Temperature (in kcal/mol): Estimate from MD (see text) and Vibrational Component Calculated in the Harmonic Approximation

	formation						dissociation					
	PBE		BLYP		B3LYP		PBE		BLYP		B3LYP	
n	MD	H	MD	H	MD	H	MD	H	MD	H	MD	H
1	−4	−4	−3	−3	−4	−3	2	1	1	1	1	1
2	−5	−6	−1	−5	abs <1	−4	abs <1	−1	−1	−1	3	−1

	formation				dissociation			
	PBE		BLYP		PBE		BLYP	
n	MD	H	MD	H	MD	H	MD	H
3	−6	−7	−3	−5	−3	−1	−2	−1
3′	−2	−8	−2	−7	4	−1	2	−1

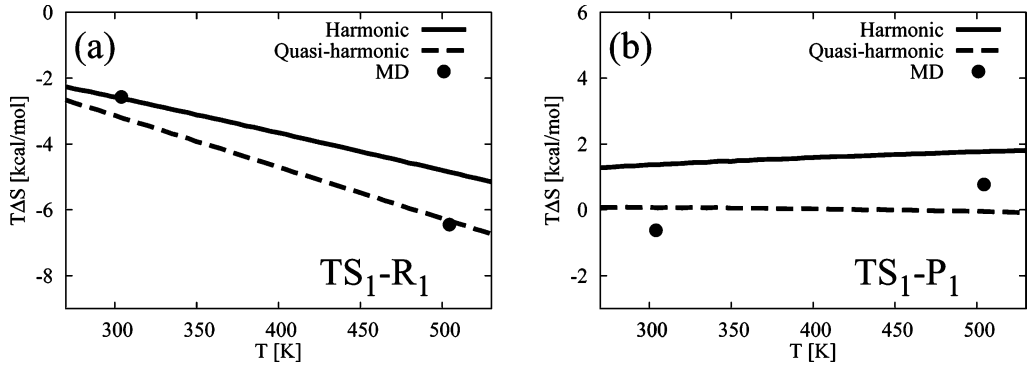

Figure 9. Entropic contribution (in kcal/mol) to free-energy barriers vs temperature: from DFT-MD (circles) and from standard calculations using harmonic (solid) and quasi-harmonic (dashed) approximations for the vibrational entropy.

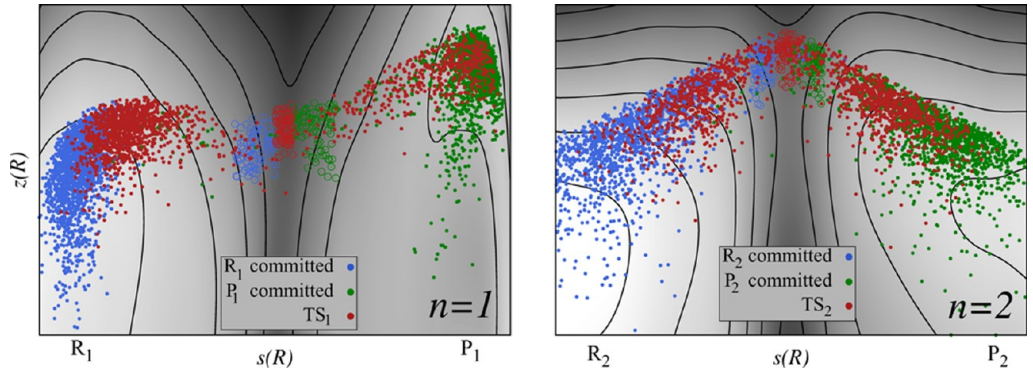

Figure 10. Committor analysis for the n = 1 and n = 2 systems: start (empty) and end (filled) points of the unbiased trajectories.

This behavior is shown in Figure 9 for the entropy term, which is also compared with the prediction of the traditional approximations. Note however that our MD values are affected by an error of ∼3 kcal/mol.

2.2.4. A Posteriori Validation of the Collective Variables. An important test of the validity of any reaction coordinates uses the committor distributions.[28] We have applied it to our CV for all systems studied; we report here the results obtained in the BLYP scheme. No remarkable change was found in the other xc-functional schemes. We considered three portions (i−iii) of the FES in the (s,z) space, near the reactant, product, and TS regions, respectively; in each of them, we selected 80 configurations pertaining to the MTD trajectory from which we shot 20 MD simulations (20 fs) each, with random initial velocities corresponding to 300 K. For example, in the case of n = 1 (Figure 10), the committor probabilities clarified that region i was committed to the reactants with p_R = 100% and region ii to the products with p_P = 98%, whereas region iii was committed to both reactants and products with p_R = 30% and p_R = 70%. For the case n = 2, also shown in Figure 10, the committor analysis for the three analogous regions resulted in p_R = 99%, p_P = 98%, and p_R = 39% and p_P = 53%, respectively. Similar results were found for the systems with three-water molecules. The validity of the reconstructed FESs for the reactions in eq 1 is thus further confirmed, and especially the localization of the TSs in the saddle-point region.

Finally, we can draw partial comparison with the MTD study of carbonic acid dissociation mentioned above.[29] Given that the trajectories calculated in ref 29 are not available, we could only investigate to what extent the CVs there chosen, namely the C−O and O−H coordination numbers, are good order parameters for the pathway that we computed with path CVs. The results (shown in the SI, Figure 4) suggest that the performance is good for the dissociation reaction, but the same

CVs lead the reactant basin to collapse into the origin of the coordinates. Therefore, these CVs cannot be employed to simulate the reverse (association) reaction.

3. CONCLUSIONS

We have studied the dynamics of the reaction of CO_2 with water molecules (formation and dissociation of carbonic acid) in the gas phase with DFT-based molecular dynamics driven by metadynamics with especially effective collective variables (path CVs[27]).

This work has given us the opportunity to establish a new protocol for this type of simulation, that relies on the reversibility of the simulated processes and exploits tools of statistical analysis, typically used for protein dynamics, to characterize the reconstructed free-energy surface with an unprecedented control of the statistical error. By ensuring robust and reproducible results, this strategy provides a seamless bridge from traditional zero-temperature calculations to a dynamical finite-temperature approach.

Although "direct dynamics" methods are especially targeted to large-scale systems in condensed phases, the possibility to compare on solid grounds the mapping of a given reaction on the PES and FES has uncovered and clarified interesting aspects of the reactions in the gas phase:

(i) In spite of significant differences found in the account of binding energies, the lowering of enthalpy barriers (catalytic effect) due to the addition of one water molecule is independent of the description of the xc-functional (be it GGA or B3LYP or M06; within one kcal/mol) and also agrees with MP2 and CCSD(T) values. This is also true, to a large extent, for the free-energy barriers evaluated within DFT.

(ii) In the case of one and two water molecules, minor differences are found in the description given by either the static or the dynamic approaches. By contrast, the system with three water molecules, especially the reactant of the formation reaction, can only be described as a statistical ensemble of quasi-degenerate configurations, and the reactions may have multiple channels. We have simulated two different pathways (as suggested by previous "static" calculations) that turn out to be competitive.

Moreover, we have been able to extract an estimate of the entropic contributions to the FE barriers and also their variation with temperature, without having to resort to an approximate decomposition into vibrational, translational, and rotational contributions.

One issue of concern for the particular systems we have considered here could be the neglect of nuclear motion quantum effects in DFT-MD. We have shown that the contribution of zero-point energy to the energy barriers is negligible, but quantum tunnelling effects may become relevant at low temperatures.[21] One way to introduce quantum effects would be combining DFT-MTD with path-integral methods as often done in unbiased DFT-MD simulations.[38]

In conclusion, we recall that often calculations in the gas phase are taken as basis for the understanding of the chemistry of CO_2 dissolved in water, and it is claimed that three or four water molecules are sufficient to model the reactions of CO_2 in the liquid. This extrapolation is based either on the closeness of the experimental data taken in aqueous solutions[39,40] with the reaction barriers calculated in the gas phase[22,26] or on the rapid convergence of the barrier with the number of water molecules, also when the molecular structures are optimized in the presence of the solvent modeled as a continuum.[25,41] Our results show indeed the rapid decrease of the catalytic effect and of the free-energy barriers toward experimental data in water.[5] However, we believe that the latter agreement is fortuitous because the reactions taking place in solution are expected to have a more complex nature and proceed via more complex paths.[4,18−20]

4. METHOD SECTION

Our DFT-based study of both PES and FES of the reactions in eq 1 used three approximations of the xc-functional: the nonempirical GGA PBE,[42] the semiempirical gradient-corrected BLYP,[43,44] and the empirical hybrid B3LYP.[45,46] All calculations employed the combined pseudopotential-plane-wave scheme as implemented in the CPMD code.[47] The DFT equations were solved for the valence electron states with standard norm-conserving angular-momentum-dependent pseudopotentials of the Martins−Troullier type.[48] When using the B3LYP xc functional, the pseudopotential was still the one derived from an all-electron BLYP calculation, which amounts to say that only the electron−electron interactions in the valence shells are treated within B3LYP. (This is the approximation currently made in all codes using hybrid functionals and plane waves as basis functions). Periodic boundary conditions were imposed corresponding to a cubic box of edge 16 Å. Being the system in the gas phase, an electrostatic decoupling scheme[49] was necessary to reduce the interactions between periodic images. Geometry optimization was made with a kinetic-energy cutoff of 100 Ry for the plane-waves basis set whereas MD was run with a cutoff of 70 Ry; we verified that this reduction changed the relevant energies at most by 2 kcal/mol, namely within the accuracy of the calculations. Our comparisons will take this difference into account explicitly.

For the sake of comparison and validation, we also report results for the PES that we have obtained in the framework of both the hybrid B3LYP[45,46] and meta-hybrid M06 functionals,[50] using all-electron schemes as implemented in NWChem,[51] with an augmented correlation consistent polarized triple-valence zeta (aug-cc-pVTZ) basis set.

4.1. PES. In our CPMD-driven calculations, we chose the limited-memory Broyden−Fletcher−Goldfarb−Shanno (L-BFGS) method for energy minimization, with no symmetry constraints, and the linear response method[52] for the determination of the vibrational frequencies.

For the search for transition state configurations, we applied a linear-scaling algorithm using the partitioned rational-function-optimizer (P-RFO).[53] In all cases, we verified that reactants (preassociation complexes) and products had only real frequencies, whereas transition states had only one imaginary frequency.

The all-electron calculations followed the standard protocol of the NWChem code,[51] namely the quasi-Newton optimization method and a modified Fletecher−Powell algorithm[54,55] for the search of transition states.

4.2. Metadynamics and FES. The Car−Parrinello[14] MD was supplemented by quenching to the Born−Oppenheimer surface every 1 ps (to within 10^{-5} Ha) and updating the ionic velocities. Equations of motion were integrated according to the velocity-Verlet algorithm with a time step of 0.1 fs. The mass for all of the fictitious dynamical electronic degrees of freedom was 500 au. The temperature was set to 300 K and controlled by a Nosé−Hoover thermostat[56,57] with $\omega = 3000$ cm^{-1}.

These calculations were driven by the PLUMED[58] routines interfaced to the CPMD code.[47]

1. Choice of the Collective Variables. Our initial choice of CVs was the number of C−O−H bridges defined as

$$n_{\mathrm{COH}} = \sum_{j\in A,k\in B} n(d_{ij})\cdot n(d_{jk}) \tag{2}$$

where i is the carbon atom and A and B are the sets of all oxygen and hydrogen atoms, respectively, and

$$n(d) = \frac{1-\left(\frac{d}{d_0}\right)^p}{1-\left(\frac{d}{d_0}\right)^{p+q}} \tag{3}$$

The function $n(d)$ is a smooth coordination function; its range and steepness are controlled by the parameters p, q, and d_0.

In order to better distinguish between reactants and products, we added a "long-range C−O coordination" variable defined in eq 3.

B. Path CVs. The path-collective variables are defined as[27]

- s, which measures the progress along the path

$$s(\mathbf{R}) = \frac{1}{\mathcal{Z}(\mathbf{R})}\sum_{\alpha=1}^{N_{\mathbf{R}^0}} \alpha\ \mathrm{e}^{-\lambda\Delta(\mathbf{R}^0_\alpha,\mathbf{R})} \tag{4}$$

- z, which measures the distance from the path

$$z(\mathbf{R}) = -\lambda^{-1}\log \mathcal{Z}(\mathbf{R}) \tag{5}$$

with

$$\mathcal{Z}(\mathbf{R}) = \sum_{\alpha=1}^{N_{\mathbf{R}^0}} \mathrm{e}^{-\lambda\Delta(\mathbf{R}^0_\alpha,\mathbf{R})} \tag{6}$$

and

$$\Delta(\mathbf{R}^0,\mathbf{R}) = \frac{2}{N_{\mathrm{at}}(N_{\mathrm{at}}-1)}\sum_{i=1}^{N_{\mathrm{at}}-1}\sum_{j=i+1}^{N_{\mathrm{at}}} (\|\mathbf{R}^0_i-\mathbf{R}^0_j\| - \|\mathbf{R}_i-\mathbf{R}_j\|)^2 \tag{7}$$

N_{at} being the number of atoms. $\{\mathbf{R}^0\}$ is a reference path from the initial to the final state of the reaction. $\Delta(\mathbf{R}^0,\mathbf{R})$ represents the distance between two configurations, and λ is related to the average distance between neighboring frames.

The initial putative reaction pathway can be suitably generated by "shooting" a few trajectories from the TS identified in the PES, or by explicit construction (e.g., linear interpolation between reactants and products). In our simulations, $\{\mathbf{R}^0\}$ consisted of about 20 frames extracted from MD trajectories initiated at the P-RFO transition state and falling either on the reactant or on the product side of the reaction. λ varied in the range 2.5−5 au^{-2} for the different systems. In particular, in the (more complicated) case of three water molecules interacting with CO_2, we ran more than one simulation and decided to include the PES minima in $\{\mathbf{R}^0\}$ to ensure that those configurations would not be missed. The importance of this addition is clear from the results (see section 2.2.3).

By construction, the s and z variables encompass all degrees of freedom and alleviate the risk of observing significantly different structures in the same region of the CV space.

We verified that the same reference path $\{\mathbf{R}^0\}$ could be satisfactorily used in all calculations; namely, it had not to be changed on passing from one xc functional scheme to the other.

One of the current drawbacks of path CVs is that they do not account for indistinguishability of atoms of the same species: chemically identical states differing only by the numbering of the atoms may end up in different regions of the FES. This amounts to a significant increase of the CV space to be explored. In order to mitigate this problem (and thus decrease the computational cost), we set a parabolic restraining wall in the z direction, which also prevents the system from escaping the reactive region.

During the simulations, Gaussians, acting directly on the CVs, were deposited along the trajectory every 50 fs (height 1.3 kcal/mol; widths of 0.4 (n = 1,2) and 0.075 (n = 3,3′) for s and 0.15 (n = 1,2) and 0.05 (n = 3,3′) for z). No extended Lagrangian formulation is employed.

2. Reconstruction and Analysis of the FES. The equilibrium free-energy surface (FES) at the simulated temperature is estimated from metadynamics simulations as

$$F(s,z) = -\frac{1}{t_{\mathrm{tot}}-t_{\mathrm{fill}}}\int_{t_{\mathrm{fill}}}^{t_{\mathrm{tot}}} \mathrm{d}t\ V_{\mathrm{G}}(s,z,t) \tag{8}$$

where $V_{\mathrm{G}}(s,z,t)$ is the sum of the Gaussian hills deposited up to time t.[35,59]

In all our simulations, the filling time t_{fill} was about 70 ps. A parallel growth of the $V_{\mathrm{G}}(s,z,t)$ profiles was observed after t_{fill}. This allowed us to estimate the statistical uncertainty of the FES profile (eq 8) both by comparing different independent simulations and by taking the averages on both halves of the $[t_{\mathrm{fill}},t_{\mathrm{tot}}]$ interval. We verified that the standard deviation was $\lesssim$2 kcal/mol on the whole relevant portion of the (s,z) space.

Free-energy basins were defined around the local minima of the FES within a window of 3 kcal/mol. TSs were defined within a small region of the CVs (see Figure 10).

Cluster analysis was made using the all-to-all distance matrix metric (eq 7) and the Gromos algorithm .[60]

Values of the relative thermodynamic quantities within a basin Ω on the FES can be computed as

$$F_\Omega = -k_{\mathrm{B}}T\ln\frac{\int_\Omega \mathrm{e}^{-\beta F(s,z)}\,\mathrm{d}s\,\mathrm{d}z}{\int \mathrm{e}^{-\beta F(s,z)}\,\mathrm{d}s\,\mathrm{d}z} \tag{9}$$

$$H_\Omega = \frac{\int_\Omega E_{\mathrm{DFT}}(s,z)\,\mathrm{e}^{-\beta F(s,z)}\,\mathrm{d}s\,\mathrm{d}z}{\int_\Omega \mathrm{e}^{-\beta F(s,z)}\,\mathrm{d}s\,\mathrm{d}z} \tag{10}$$

$$T\Delta S_\Omega = \Delta H_\Omega - \Delta F_\Omega \tag{11}$$

where E_{DFT} is the total energy of the system.

■ ASSOCIATED CONTENT

Supporting Information

From PES calculations: Geometric charcateristics of reactants, transition states and products; BLYP binding energies compared with BLYP-D; characteristics of the water dimer and trimer calculated within all schemes considered here; ZPE contribution to binding energies and enthalpy barriers. From FES calculations: entropy contribution to free-energy barriers; free-energy profiles and free-energy surfaces for all cases studied; additional cluster analysis and more on CV validation (as mentioned in the text). This material is available free of charge via the Internet at http://pubs.acs.org.

■ AUTHOR INFORMATION

Corresponding Author

*E-mail: wanda.andreoni@epfl.ch.

Notes

The authors declare no competing financial interest.

■ ACKNOWLEDGMENTS

The financial support for CADMOS and for the Blue Gene/P system is provided by the Canton of Geneva, the Canton Vaud, the Hans Wilsdorf foundation, the Louis-Jeantet foundation, the University of Geneva, the University of Lausanne, and the Ecole Polytechnique Fédérale de Lausanne.

■ REFERENCES

(1) Tossell, J. *Environ. Sci. Technol.* **2009**, *43*, 2575−2580.
(2) Puxty, G.; Rowland, R.; Allport, A.; Yang, Q.; Bown, M.; Burns, R.; Maeder, M.; Attalla, M. *Environ. Sci. Technol.* **2009**, *43*, 6427−6433.
(3) Chen, W.; Hou, Y.; Hung, C. *Appl. Energy* **2011**, *92*, 185−193.
(4) Adamczyk, K.; Premont-Schwarz, M.; Pines, D.; Pines, E.; Nibbering, E. *Science* **2009**, *326*, 1690−1694.
(5) Wang, X.; Conway, W.; Burns, R.; McCann, N.; Maeder, M. *J. Phys. Chem. A* **2010**, *114*, 1734−1740.
(6) Hänggi, P.; Talkner, P.; Borkovec, M. *Rev. Mod. Phys.* **1990**, *62*, 251−341.
(7) Truhlar, D. G.; Garrett, B. C.; Klippenstein, S. J. *J. Phys. Chem.* **1996**, *100*, 12771−12800.
(8) Porter, R. N. *Annu. Rev. Phys. Chem.* **1974**, *25*, 317−355.
(9) Schatz, G. C. *Annu. Rev. Phys. Chem.* **1988**, *39*, 317−340.
(10) Light, J. C.; Zhang, D. H. *Faraday Discuss.* **1998**, *110*, 105−118.
(11) Clary, D. *Proc. Natl. Acad. Sci. U. S. A.* **2008**, *105*, 12649−12653.
(12) Voth, G.; Chandler, D.; Miller, W. *J. Chem. Phys.* **1989**, *91*, 7749−7760.
(13) Cramer, C. J.; Truhlar, D. G. *Chem. Rev.* **1999**, *99*, 2161−2200.
(14) Car, R.; Parrinello, M. *Phys. Rev. Lett.* **1985**, *55*, 2471−2474.
(15) Laio, A.; Parrinello, M. *Proc. Natl. Acad. Sci. U. S. A.* **2002**, *99*, 12562−12566.
(16) Laio, A.; Gervasio, F. *Rep. Prog. Phys.* **2008**, *71*, 126601−126622.
(17) Barducci, A.; Bonomi, M.; Parrinello, M. *Comput. Mol. Sci.* **2011**, *1*, 826−843.
(18) Stirling, A.; Papai, I. *J. Phys. Chem. B* **2010**, *114*, 16854−16859.
(19) Stirling, A. *J. Phys. Chem. B* **2011**, *115*, 14683−14687.
(20) Galib, M.; Hanna, G. *J. Phys. Chem. B* **2011**, *115*, 15024−15035.
(21) Loerting, T.; Tautermann, C.; Kroemer, R. T.; Kohl, I.; Hallbrucker, A.; Mayer, E.; Liedl, K. R. *Angew. Chem., Int. Ed.* **2000**, *39*, 891−894.
(22) Tautermann, C. S.; Voegele, A. F.; Loerting, T.; Kohl, I.; Hallbrucker, A.; Mayer, E.; Liedl, K. R. *Chem.—Eur. J.* **2002**, *8*, 66−73.
(23) Lewis, M.; Glaser, R. *J. Phys. Chem. A* **2003**, *107*, 6814−6818.
(24) Jena, N.; Mishra, P. *Theor. Chem. Acc.* **2005**, *114*, 189−199.
(25) Nguyen, M. T.; Matus, M. H.; Jackson, V. E.; Ngan, V. T.; Rustad, J.; Dixon, D. A. *J. Phys. Chem. A* **2008**, *112*, 10386−10398.
(26) Baltrusaitis, J.; Grassian, V. H. *J. Phys. Chem. A* **2010**, *114*, 2350−2356.
(27) Branduardi, D.; Gervasio, F. L.; Parrinello, M. *J. Chem. Phys.* **2007**, *126*, 054103−054112.
(28) Bolhuis, P.; Chandler, D.; Dellago, C.; Geissler, P. *Annu. Rev. Phys. Chem.* **2002**, *53*, 291−318.
(29) Kumar, P. P.; Kalinichev, A. G.; Kirkpatrick, R. J. *J. Chem. Phys.* **2007**, *126*, 204315−204322.
(30) Lin, C.-L.; Chu, S.-Y. *J. Chin. Chem. Soc.* **2002**, *49*, 777−781.
(31) Ireta, J.; Neugebauer, J.; Scheffler, M. *J. Phys. Chem. A* **2004**, *108*, 5692−5695.
(32) Grimme, S. *J. Comput. Chem.* **2004**, *25*, 1463−1473.
(33) Grimme, S. *J. Comput. Chem.* **2006**, *27*, 1787−1799.
(34) Geissler, P. L.; Dellago, C.; Chandler, D. *J. Phys. Chem. B* **1999**, *103*, 3706−3710.
(35) Laio, A.; Rodriguez-Fortea, A.; Gervasio, F. L.; Ceccarelli, M.; Parrinello, M. *J. Phys. Chem. B* **2005**, *109*, 6714−6721.
(36) Branduardi, D.; De Vivo, M.; Rega, N.; Barone, V.; Cavalli, A. *J. Chem. Theory Comput.* **2011**, *7*, 539−543.
(37) McQuarrie, D. A.; Simon, J. D. *Molecular Thermodynamics*; University Science Books: Sausalito, CA, 1999.
(38) Marx, D.; Parrinello, M. *Z. Phys. B* **1994**, *95*, 143−144.
(39) Magid, E.; Turbeck, B. *Biochim. Biophys. Acta* **1968**, *165*, 515−524.
(40) Pocker, Y.; Bjorkquist, D. *J. Am. Chem. Soc.* **1977**, *99*, 6537−6543.
(41) Nguyen, M. T.; Raspoet, G.; Vanquickenborne, L. G.; Van Duijnen, P. T. *J. Phys. Chem. A* **1997**, *101*, 7379−7388.
(42) Perdew, J. P.; Burke, K.; Ernzerhof, M. *Phys. Rev. Lett.* **1997**, *78*, 1396−1396.
(43) Becke, A. D. *Phys. Rev. A* **1988**, *38*, 3098−3100.
(44) Lee, C.; Yang, W.; Parr, R. G. *Phys. Rev. B* **1988**, *37*, 785−789.
(45) Stephens, P. J.; Devlin, F. J.; Chabalowski, C. F.; Frisch, M. J. *J. Phys. Chem.* **1994**, *98*, 11623−11627.
(46) Vosko, S. H.; Wilk, L.; Nusair, M. *Can. J. Phys.* **1980**, *58*, 1200−1211.
(47) *CPMD*; IBM Corp.: Armonk, NY, 1990−2012; MPI für Festkörperforschung Stuttgart: Stuttgart, 1997−2001.
(48) Troullier, N.; Martins, J. L. *Phys. Rev. B* **1991**, *43*, 1993−2006.
(49) Martyna, G. J.; Tuckerman, M. E. *J. Chem. Phys.* **1999**, *110*, 2810−2821.
(50) Zhao, Y.; Truhlar, D. *Theor. Chem. Acc.* **2008**, *120*, 215−241.
(51) Valiev, M.; Bylaska, E.; Govind, N.; Kowalski, K.; Straatsma, T.; Dam, H. V.; Wang, D.; Nieplocha, J.; Apra, E.; Windus, T.; de Jong, W. *Comput. Phys. Commun.* **2010**, *181*, 1477−1489.
(52) Baroni, S.; de Gironcoli, S.; Dal Corso, A.; Giannozzi, P. *Rev. Mod. Phys.* **2001**, *73*, 515−562.
(53) Billeter, S. R.; Curioni, A.; Andreoni, W. *Comput. Mater. Sci.* **2003**, *27*, 437−445.
(54) Shanno, D. F. *Math. Comput.* **1970**, *24*, 647−656.
(55) Fletcher, R. *Comput. J.* **1970**, *13*, 317−322.
(56) Nosé, S. *J. Chem. Phys.* **1984**, *81*, 511−519.
(57) Hoover, W. G. *Phys. Rev. A* **1985**, *31*, 1695−1697.
(58) Bonomi, M.; Branduardi, D.; Bussi, G.; Camilloni, C.; Provasi, D.; Raiteri, P.; Donadio, D.; Marinelli, F.; Pietrucci, F.; Broglia, R. A.; Parrinello, M. *Comput. Phys. Commun.* **2009**, *180*, 1961−1972.
(59) Crespo, Y.; Marinelli, F.; Pietrucci, F.; Laio, A. *Phys. Rev. E* **2010**, *81*, 055701−055704.
(60) Daura, X.; Gademann, K.; Jaun, B.; Seebach, D.; van Gunsteren, W.; Mark, A. *Angew. Chem., Int. Ed.* **1999**, *38*, 236−240.